Real-Time Stabilization of a Small Three-Rotor Aircraft

SERGIO SALAZAR-CRUZ
FARID KENDOUL
ROGELIO LOZANO, Member, IEEE
ISABELLE FANTONI, Member, IEEE
Heudiasyc Laboratory
France

This paper describes the design and control algorithm of an original configuration for a small aerial vehicle having three rotors with fixed-pitch propellers. The mechanism of forces and moments generation is described and compared with other vertical take-off and landing (VTOL) vehicles. A mathematical model of the body-forces generation process as well as the 6-DOF (degree of freedom) krotorcraft dynamics is presented. A stabilization algorithm is proposed which takes into account the input amplitude bounds as well as nonlinear couplings in the three-rotor dynamics. The performance of the control strategy is shown in real-time experiments.

Manuscript received October 13, 2006; revised February 7 and March 3, 2007; released for publication June 11, 2007.

IEEE Log No. T-AES/44/2/926559.

Refereeing of this contribution was handled by R. C. Michelson.

Authors' address: Heudiasyc, UMR CNRS 6599, Université de Technologie de Compiègne, Centre de Recherches de Royallieu, BP20529 60205, Compiègne, Cedex, France, E-mail: (ifantoni@hds.utc.fr).

I. INTRODUCTION

Unmanned aerial vehicles (UAVs) are defined as pilotless flying vehicles. These self-propelled air machines are either remotely controlled or are capable of conducting autonomous operations. Early UAVs were developed just after the end of the Second World War but since then, very little has been done on the development of new configurations. In the last decade, considerable research has been performed on the design, analysis, and operation of autonomous VTOL aircraft. Rotary-wing vehicles have a distinct advantage over fixed-wing aircraft especially in an urban environment, where hover capability is helpful. There is an increased interest in the deployment of autonomous helicopters for military applications. They have been used in the past years over a wide range of military missions. Nevertheless, UAVs may also represent a promising and cost-effective alternative to manned aircraft for a large number of civil aviation applications.

Design of small autonomous and operational UAVs involves many problems related to limited payload, energy and flight endurance, embedded sensors, navigation, etc. Control systems have to be reliable, efficient and robust against environment perturbations. The stabilization control problem of autonomous helicopter is challenging since the vehicle dynamics are highly nonlinear and coupled with unknown disturbances.

The control of a rotorcraft in hover has been dealt with from different points of view namely, artificial neural networks schemes [1], linear controllers [2], sliding mode control [3], backstepping [4] and forwarding methodologies [5], adaptive control [6], feedback linearization [7], passivity-based control [8], nonlinear control with bounded inputs [9–12]. For more details, refer to [13] and [14] which address intelligent control architectures for UAVs including mission planning, trajectory generation, and vehicle navigation.

In this paper, we present an innovative small aircraft with three rotors and non-cyclic propellers. We present the nonlinear model and design a control algorithm. This low-cost configuration is able to perform vertical take-off and landing (VTOL), hovering, and horizontal flight. Three-rotor aircraft steering maneuvers are performed by changing the speed of the three rotors, thereby eliminating linkages, moveable rudder or elevator, and many of the parts which make a normal helicopter expensive. The three-rotor aircraft is suitable for the miniaturization required for small UAVs, and it results in a simple mechanical realization. Therefore, the three-rotor-based configuration represents an interesting alternative solution to small VTOL UAVs since it combines the advantages of standard helicopters and quadrotor rotorcraft (see Section II).

The idea of designing three-rotor aircraft is not new. In 1948, the three-rotor "Cierva Air Horse" helicopter made its maiden flight and was displayed at the Farnborough Air Show. It could carry 24 passengers and was at that time the world's largest and heaviest helicopter. In 2002, BRAUN MODELLTECHNIK Inc. designed and commercialized a small three-rotor helicopter called Tribelle.

This paper is organized as follows. Section II presents a comparison between the three-rotor aircraft with respect to other configurations. Section III describes a nonlinear model for the three-rotor aircraft dynamics. Section IV is devoted to the design of an autopilot for autonomous stabilization of the proposed configuration considering the translation-rotation coupling and inputs boundedness. The proposed controller is based on the sum of saturation functions [15]. Section V shows the testbed and the experimental results. Conclusions are finally given in Section VI.

II. THREE-ROTOR AIRCRAFT PERFORMANCE

Recently, there has been an increasing interest in the development of small autonomous rotary-wing vehicles for military and civil applications, especially in urban and indoor environments. The well-known rotorcraft in the family of small rotary-wings UAVs are conventional helicopters [2, 16] and four-rotor aircraft [3, 11, 17, 18]. For more details and information on other UAVs platforms and technologies, refer to [14] and [19].

In the following, we briefly describe the advantages and drawbacks of each configuration and show that the three-rotor aircraft is a promising alternative to small VTOL UAVs. Indeed, it presents a good trade-off between helicopters (2 rotors) and quadrotor rotorcraft (4 rotors).

A. Conventional Helicopters (2 rotors)

The classical helicopter is characterized by a main rotor which provides the total thrust, and a tail rotor for compensating the reactive anti-torque due to the main rotor. The lateral force generated by the tail rotor is used for yaw control, and does not participate to the total thrust generation. So, the energy spent by the tail rotor can be considered as a passive or lost energy. Roll and pitch torques are generated by the thrust vectoring procedure using two servomotors for blades pitching. More precisely, blades on a helicopter are pitched, or angled, in different ways to control the orientation and direction of the craft movement.

The main advantage of this configuration is its high manoeuvrability and good performance during forward flight. Indeed, unmanned helicopters are versatile machines that can perform aggressive maneuvers.

B. Quadrotor Rotorcraft (4 rotors)

The four-rotor-based mechanism is generally used for small UAVs like the Draganfly rotorcraft. The front and the rear motors rotate counterclockwise while the other two rotate clockwise, then, gyroscopic effects and aerodynamic torques tend to cancel in trimmed flight. The main thrust and control torques are obtained by controlling the angular speed of the four rotors, without using any servomechanism. So, the maintenance of the quadrotor rotorcraft is relatively simple as compared with a classical helicopter.

In this type of rotorcraft, the yaw movement is obtained by increasing (decreasing) the speed of the front and rear motors while decreasing (increasing) the speed of the lateral motors. Since the yaw torque is related to drag fan torques (aerodynamical torques), it is thus very difficult to express the yaw torque magnitude in terms of original control inputs (rotors angular velocities w_i). In fact, aerodynamical relations modelling the yawing torque are complex and not well known. Then, they are generally approximated by simplified expressions, resulting in significant modeling errors. This means that the control of the quadrotor direction (or yaw angle) will result in significant error which is not appropriate for cluttered and indoor environments. Moreover, the yawing torque is obtained by accelerating two motors and decelerating the two others.

C. Three-rotor Aircraft (3 rotors)

Over the past few years, we have worked on the above two mentioned configurations [20, 8, 21]. After many efforts to design an effective flying machine which combines the advantages of conventional helicopters and quadrotor vehicles, we have proposed the three-rotor aircraft as an alternative solution to small VTOL UAVs (Fig. 1).

The mechanical structure of the proposed three-rotor aircraft is as simple as the conception of the quadrotor vehicle. Indeed, the absence of mechanical linkages and swashplate makes it more robust and easier to repair than classical helicopters, and increases its life duration. The originality of the configuration lies in its control mechanism for generating the required control forces and torques. The three-rotor aircraft consists of two body-fixed rotors and a tail tilting rotor with fixed-angle blades. The two front rotors rotate in opposite directions, thereby eliminating reactive anti-torques. Since the two front rotors are powered by two independent motors, their angular velocities can be controlled to produce the main thrust as well as the roll torque. The tail rotor can be tilted laterally (see Fig. 2) using a servo-motor in order to provide the yawing torque. Finally, the pitch torque is obtained by varying the angular speed of the tail rotor.

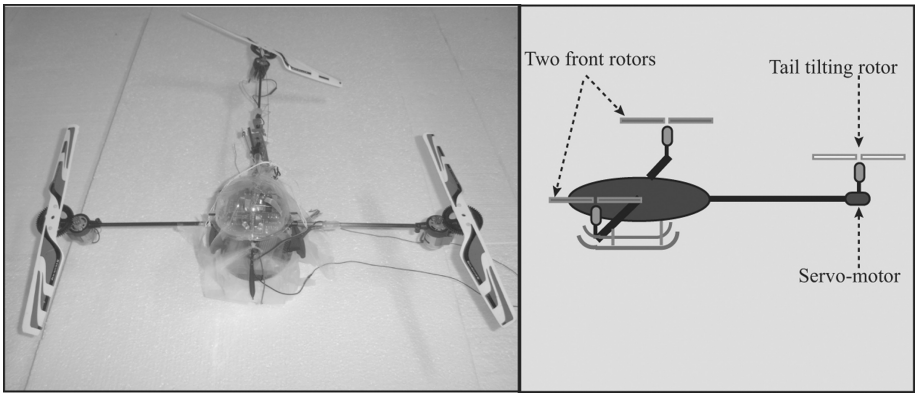

Fig. 1. Three-rotor aircraft.

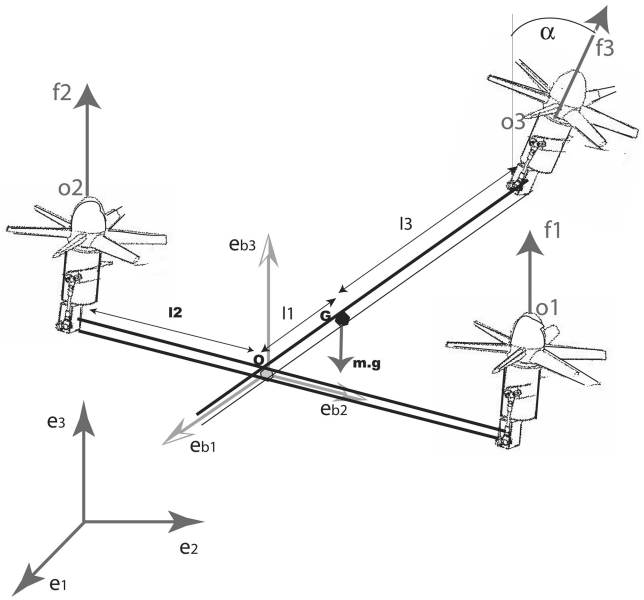

Fig. 2. Three-rotor rigid body and associated reference frames.

Contrary to the quadrotor aircraft, the yawing torque generated by the three-rotor helicopter is well understood and well modeled since it is expressed as the product of the lateral component of f_3 and the distance l_3.

During manual flight tests the three-rotor aircraft performs the translational flight better than the quadrotor aircraft.

III. THREE-ROTOR AIRCRAFT MODEL

The full model of a helicopter involving the flexibility of rotors, fuselage aerodynamics and actuators dynamics is very complex [22]. For control practical purposes, the aerial robot can be considered as a rigid body evolving in a 3D space [23] with a mechanism for generating the control force and torque vectors.

The body forces and moments acting on the airframe are the rotation speed of each motor w_i, ($i = 1,2,3$) and the tilt angle (α) of the tail rotor.

The force vector generated by propellers is expressed in the rigid body frame $\mathcal{B} = (e_{b1}, e_{b2}, e_{b3})$ (see Fig. 2) as

$$F_b = (0, f_3 \sin\alpha, f_1 + f_2 + f_3 \cos\alpha)^T. \tag{1}$$

Let us denote by (O_1, O_2, O_3) the application points of the forces (f_1, f_2, f_3), respectively. Then, the torque vector $M_F^{\mathcal{B}}$ induced by these forces with respect to the mass center G can be expressed in $\mathcal{B}$ as follows, (see Fig. 2):

$$\begin{aligned} M_F^{\mathcal{B}} = {} & \overrightarrow{GO}_1 \times (0,0,f_1) + \overrightarrow{GO}_2 \times (0,0,f_2) \\ & + \overrightarrow{GO}_3 \times (0, f_3 \sin\alpha, f_3 \cos\alpha). \end{aligned} \tag{2}$$

The components of $M_F^{\mathcal{B}}$ in the body frame are

$$M_F^{\mathcal{B}} = \begin{pmatrix} l_2(f_1 - f_2) \\ -l_1(f_1 + f_2) + l_3 f_3 \cos\alpha \\ -l_3 f_3 \sin\alpha \end{pmatrix}. \tag{3}$$

The distances l_i ($i = 1,2,3$) are defined in Fig. 2.

The drag force for each of the blades is given as

$$\begin{aligned} Q_i &= (0,0,(-1)^i \kappa \omega_i^2)^T, \qquad i = 1,2 \\ Q_3 &= (0, \kappa\omega_3^2 \sin\alpha, \kappa\omega_3^2 \cos\alpha)^T \end{aligned} \tag{4}$$

where κ is a positive constant characterizing the propeller aerodynamics [22] and ω_i is the angular velocity of rotor i.

Furthermore, there exists other parasitic moments specific to the three-rotor helicopter. Indeed, tilting the tail rotor laterally results in additional small moment. An adverse reaction moment appears when precessing the tail rotor laterally. It depends essentially on the tail rotor inertia I_p and on the tilt angle acceleration $\ddot{\alpha}$. This moment acts as a rolling torque and can be expressed in $\mathcal{B}$ as [4]

$$M_{a.r} = (-I_p \ddot{\alpha}, 0, 0)^T. \tag{5}$$

The gyroscopical effect of tilting the tail rotor induces other moments. Tilting propellers around the e_{b1}-axis, creates a gyroscopic moment which is perpendicular to this axis and to its spin axis. Indeed,

this moment is defined by the cross product of the kinetic moment ($I_r\omega_3$) of the propeller and the tilt velocity vector. It can be written in the form [4]

$$M_{gy} = (0, I_r\omega_3\dot{\alpha}\cos\alpha, -I_r\omega_3\dot{\alpha}\sin\alpha)^T \tag{6}$$

with I_r is the tail rotor inertia moment with respect to its spin axis.

Thus, the complete expression of the total torque vector τ acting on helicopter frame is obtained by summing (3)–(4)

$$\tau = \begin{pmatrix} l_2(f_1 - f_2) - I_p\ddot{\alpha} \\ -l_1(f_1 + f_2) + l_3 f_3\cos\alpha + I_r\omega_3\dot{\alpha}\cos\alpha + \kappa\omega_3^2\sin\alpha \\ -l_3 f_3\sin\alpha - I_r\omega_3\dot{\alpha}\sin\alpha + \kappa(\omega_2^2 - \omega_1^2 + \omega_3^2\cos\alpha) \end{pmatrix}. \tag{7}$$

For simplicity let us split the torque vector into two parts: the nominal torque vector denoted τ_b (see (8)), and a parasitic torque vector τ_{tail} mainly induced by the tail tilting rotor (see (9)).

$$\tau_b = \begin{pmatrix} l_2(f_1 - f_2) \\ -l_1(f_1 + f_2) + l_3 f_3\cos\alpha \\ -l_3 f_3\sin\alpha \end{pmatrix} \tag{8}$$

$$\tau_{\text{tail}} = \begin{pmatrix} -I_p\ddot{\alpha} \\ I_r\omega_3\dot{\alpha}\cos\alpha + \kappa\omega_3^2\sin\alpha \\ -I_r\omega_3\dot{\alpha}\sin\alpha + \kappa(\omega_2^2 - \omega_1^2 + \omega_3^2\cos\alpha) \end{pmatrix}. \tag{9}$$

The magnitude of the remaining perturbing torques in (9) depends on tail rotor angular velocity ω_3, tail rotor inertias (I_p,I_r), and tilt angle α and its time derivatives. Let us recall that the major thrust is provided by the two front motors, then, ω_3 is relatively small compared with ω_1 and ω_2. Tail rotor inertias (I_p,I_r) of the three-rotor helicopter are very small. Furthermore, the synthesized control strategy aims at fast stabilization of the yaw angle (see Section IV) which results in small values of $(\alpha, \dot{\alpha}, \ddot{\alpha})$. The basic idea of this approach is to reduce the parasitic effects of the tail rotor tilting when controlling the remaining state variables. Thus, the parasitic small body moments in (9) will allow arbitrary (though bounded) control action and will converge to zero when the yaw angle is stabilized.

However, the most challenging issue in controlling the three-rotor helicopter is the lateral force (1) generated from tilting the tail rotor. Indeed, the force vector F_b in (1) and the torque vector τ_b in (8) are coupled through the lateral force $f_3\sin\alpha$.

$$F_b = (0, 0, u)^T + N\tau_b \tag{10}$$

with

$$N = \begin{pmatrix} 0 & 0 & 0 \\ 0 & 0 & -1/l_3 \\ 0 & 0 & 0 \end{pmatrix} \tag{11}$$

and

$$u = f_1 + f_2 + f_3\cos\alpha \tag{12}$$

is the body-vertical component of the force vector which is considered as the nominal control force.

REMARK 1 Note that the change of input variables in (12) and (8) defines a diffeomorphism, i.e., the original control inputs (f_1, f_2, f_3, α) can be recovered from (u, τ_b^T) which are computed from the control law.

The equations of motion for a rigid body subject to a body force $F^{\mathcal{B}} \in \mathbb{R}^3$ and a torque $\tau_b \in \mathbb{R}^3$ applied to the center of mass G and specified with respect to the body coordinate frame $\mathcal{B}$ (see Fig. 2) are given by the following Newton-Euler equations in $\mathcal{B}$, [2, 8, 24]

$$\begin{aligned} m\dot{v}^{\mathcal{B}} + \Omega \times mv^{\mathcal{B}} &= F^{\mathcal{B}} \\ J\dot{\Omega} + \Omega \times J\Omega &= \tau_b \end{aligned} \tag{13}$$

where $v^{\mathcal{B}} \in \mathbb{R}^3$ and $\Omega \in \mathbb{R}^3$ are, respectively, the body velocity vector and the body angular velocity vector expressed in the body frame $\mathcal{B}$. $m \in \mathbb{R}$ is the mass, and $J \in \mathbb{R}^{3\times3}$ is an inertial matrix expressed in $\mathcal{B}$. $F^{\mathcal{B}}$ is the gravity force mg and the body-lift vector F_b generated by propellers.

The position $\xi = (x, y, z)^T \in \mathbb{R}^3$ and the velocity of the helicopter center of gravity $v^{\mathcal{I}} \in \mathbb{R}^3$ can be also expressed in the inertial frame $\mathcal{I} = (e_1, e_2, e_3)$. Let $R \in SO(3)$ be the rotational matrix of the body axis relative to the spatial axes. R can be obtained using Euler angles $\eta = (\psi, \theta, \phi)^T$ which are, respectively, the yaw, pitch and roll:

$$R = \begin{bmatrix} c_\theta c_\psi & c_\theta s_\psi & -s_\theta \\ s_\phi s_\theta c_\psi - c_\phi s_\psi & s_\phi s_\theta s_\psi + c_\phi c_\psi & s_\phi c_\theta \\ c_\phi s_\theta c_\psi + s_\phi s_\psi & c_\phi s_\theta s_\psi - s_\phi c_\psi & c_\phi c_\theta \end{bmatrix}. \tag{14}$$

Note that $R^{-1} = R^T$, $\det(R) = 1$ and s_ϕ and c_ϕ represent the $\sin\phi$ and $\cos\phi$, respectively. Applying this transformation on (13) we get, [25]

$$\begin{aligned} m\ddot{\xi} &= RF_b - mge_3 \\ J\dot{\Omega} + \Omega \times J\Omega &= \tau_b. \end{aligned} \tag{15}$$

Let us recall the kinematic relationship between the generalized velocities $\dot{\eta} = (\dot{\psi}, \dot{\theta}, \dot{\phi})^T$ and the angular velocity Ω

$$\Omega = W\dot{\eta} \tag{16}$$

where W is called the Euler matrix and is given by [17, 24]

$$W(\eta) = \begin{bmatrix} 0 & -s_\psi & c_\psi c_\theta \\ 0 & c_\psi & s_\psi c_\theta \\ 1 & 0 & -s_\theta \end{bmatrix}. \tag{17}$$

In order to obtain a system structure that is suitable for control purpose, we will transform system (15). Substituting (16) into (15), we obtain

$$\begin{aligned} m\ddot{\xi} &= RF_b - mge_3 \\ JW\ddot{\eta} + J\dot{W}\dot{\eta} + W\dot{\eta} \times JW\dot{\eta} &= \tau_b. \end{aligned} \tag{18}$$

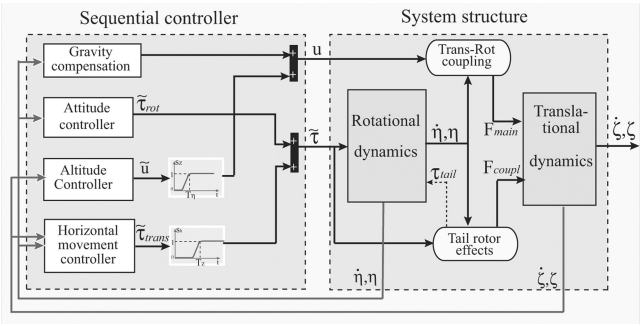

Fig. 3. System structure and control strategy diagram.

IV. SATURATING FUNCTIONS-BASED SEQUENTIAL CONTROL STRATEGY

The control objective is to express the four inputs ($u \in \mathbb{R}, \tau_b \in \mathbb{R}^3$) in terms of ($\dot{\xi}, \xi, \dot{\eta}, \eta$) in order to stabilize the system (18) considering the rotation-translation coupling as well as actuators limitations.

The three-rotor aircraft has a nonlinear underactuated dynamic model (18), where the rotation couples and the translation are coupled through the matrix R and the force vector $RN\tau_b$ generated by tilting the tail rotor. The proposed framework for stabilizing the underactuated system (18) while considering inputs boundedness and translation-rotation coupling is the design of a robust controller using forwarding approach with three time-scale controls. In fact, our control strategy takes advantage of the structure of the three-rotor helicopter model, and it is obtained in three sequential steps: 1) partial-control[1] of the vehicle's attitude (fast dynamics), 2) non-aggressive[2] control of the altitude z, 3) stabilization of the horizontal movement (slow dynamics) using thrust vectoring procedure.[3] This proposed control strategy results in a physical-intuitive procedure to stabilize a VTOL aircraft.

More precisely, the developed controller is based on the sum of saturating functions whose objective is to sequentially bound control inputs and state variables in an appropriate priority order. This control law is motivated by its ability to handle coupling terms between rotation and translation as well as control inputs boundedness. The basic idea behind this control strategy is to reduce the effects of nonlinear coupling terms by bounding the coupling force vector ($F_{\text{coupl}} = RN\tau_b$) by an arbitrary small constant (see Fig. 3 and Appendix B).

[1]Keeping the Euler angles in an arbitrary small neighborhood of the origin.

[2]Since the thrust vector is almost vertical after attitude control, then, the altitude control could be achieved with an amplitude of u slightly higher than the vehicle's weight.

[3]The thrust vector is effectively oriented in the desired direction by commanding small changes to the helicopter attitude.

Thus, the control law is constructed in three steps "by" viewing the three-rotor aircraft model as three connected subsystems. We note that the convergence property is proven for the whole connected system with considering the perturbing coupling term $RN\tau_b$.

The three main steps of the proposed controller are illustrated in Fig. 3.

After describing the controller principle, we present the mathematical analysis proving the asymptotic stability of the whole closed-loop system.

Let us first, consider the following change of variables

$$\tau_b = J\dot{W}\dot{\eta} + W\ddot{\eta} \times JW\dot{\eta} + (JW)\tilde{\tau} \tag{19}$$

with $\tilde{\tau} = (\tilde{\tau}_\psi, \tilde{\tau}_\theta, \tilde{\tau}_\phi)^T$ is the new control torque vector.

Thus, system (18) becomes

$$\begin{aligned} m\ddot{\xi} &= u(Re_3) - mge_3 + (Re_2)f(\eta, \dot{\eta}, \tilde{\tau}) \\ \ddot{\eta} &= \tilde{\tau} \end{aligned} \tag{20}$$

with

$$f(\eta, \dot{\eta}, \tilde{\tau}) = \frac{-1}{l_3}((j_2 - j_1 - j_3)\dot{\phi}\dot{\theta}c_\theta - j_3 s_\theta \tilde{\tau}_\phi + j_3\tilde{\tau}_\psi). \tag{21}$$

(j_1, j_2, j_3) are the diagonal elements of the inertia matrix J.

Notations and Definitions: We denote $|X| \in \mathbb{R}^n$ as a positive vector which is composed of the absolute value of each component of $X \in \mathbb{R}^n$, i.e., $|X| = (|x_1|, |x_2|, \ldots, |x_n|)^T$. In the following sections, for $|X| \in \mathbb{R}^n$ and $|Y| \in \mathbb{R}^n$, the notation $|X| > (<)|Y|$ means that $|x_i| > (<)|y_i|$, $\forall i \in \{1, 2, \ldots, n\}$.

We define a linear saturation function from $\mathbb{R}$ to $\mathbb{R}$ as follows: $\sigma_\lambda(x) = \text{sign}(x)$. $\min(|x|, \lambda)$ where λ is a real positive constant called the saturation level.

A vector saturation function $\sigma_a : \mathbb{R}^3 \to \mathbb{R}^3$ can be defined as

$$\sigma_a(X) = (\sigma_{a_1}(x_1), \sigma_{a_2}(x_2), \sigma_{a_3}(x_3))^T$$

with $(a_1, a_2, a_3)^T = a$ and a_i are real positive constants.

A. Step 1. Attitude Control

Let us write the control vector $\tilde{\tau}$ as a sum of two terms:

$$\tilde{\tau} = \tilde{\tau}_{\text{rot}}(\dot{\eta}, \eta) + s_h(\eta, z)\tilde{\tau}_{\text{trans}}(\dot{\eta}, \eta, \dot{\xi}, \xi) \tag{22}$$

where the first term $\tilde{\tau}_{\text{rot}}$ is used for attitude control and the second term $\tilde{\tau}_{\text{trans}}$ is used for horizontal movement control. Function $0 \leq s_h(\eta, z) \leq 1$ is a continuous non-decreasing real-valued function which is used for establishing the sequential control procedure described in Section IV.

Let us consider the subsystem representing the rotational dynamics

$$\ddot{\eta} = \tilde{\tau}. \tag{23}$$

In this section, we control the orientation variables η and $\dot{\eta}$ in such a way that they remain in a small neighborhood of the origin using the torque vector $\tilde{\tau}_{\text{rot}}$ and considering the constraint $|\tilde{\tau}| \le \tilde{\tau}_{\max}$.

PROPOSITION 1 *Consider system* (23) *and two positive constant vectors* $(a,b) \in \mathbb{R}^3 \times \mathbb{R}^3$. *If we choose*

$$\begin{aligned} \tilde{\tau}_{\text{rot}} &= -\sigma_a(\dot{\eta}) - \sigma_b(\dot{\eta} + \eta) \\ a > b + \max(\tilde{\tau}_{\text{trans}}) \quad &\text{and} \quad b > \max(\tilde{\tau}_{\text{trans}}) \end{aligned} \tag{24}$$

then, $\exists T_\eta \ge 0$, *such that*

$$|\dot{\eta}| \le a \qquad \text{and} \qquad |\eta| \le b, \qquad \forall \quad t \ge T_\eta. \tag{25}$$

Furthermore, if we set $\tilde{\tau}_{\text{trans}} \equiv 0$, *then* $\dot{\eta}$ *and* η *will exponentially converge to zero.*

The proof of Proposition 1 is given in Appendix A.

From (14) and (20), we can note that the main force vector $F_{\text{main}} = u(Re_3)$ is independent of the yaw angle ψ while the coupling force $F_{\text{coupl}} = (Re_2)f(\eta,\dot{\eta},\tilde{\tau})$ depends on the yaw angle. Therefore, in this step we also stabilize the yaw angle at 0 by choosing $\tilde{\tau}_{\text{trans}} e_3 \equiv 0$. Thus, we have $\lim_{t\to\infty} \psi = 0$ and $\lim_{t\to\infty} \tilde{\tau} e_3 = \lim_{t\to\infty} \tilde{\tau}_\psi = 0$, thereby decreasing the magnitude of the coupling force F_{coupl} and the perturbing term τ_{tail} in (9).

B. Step 2. Altitude Control

From Proposition 1, we have $|\phi| \le b_\phi$, $|\theta| \le b_\theta$, $\psi \approx 0$ and $\tilde{\tau}_\psi \approx 0$ $\forall t \ge T_\eta$. So, projecting the translational dynamics (20) on the vertical z-axis with considering ($\psi \approx 0$, $\tilde{\tau}_\psi \approx 0$) yields to

$$m\ddot{z} = u\cos\theta\cos\phi - mg - \sin\phi f(\dot{\eta},\eta,\tilde{\tau}_\phi). \tag{26}$$

The gravity force can be compensated by considering the following feedback linearization

$$u = \frac{m s_z(\eta)\tilde{u} + mg + \sin\phi f(\dot{\eta},\eta,\tilde{\tau}_\phi)}{\cos\theta\cos\phi}. \tag{27}$$

In order to avoid singularities in (27), b_ϕ and b_θ are chosen to be smaller than $\pi/2$.

Then, (26) becomes linear: $\ddot{z} = s_z(\eta)\tilde{u}$ with $\tilde{u}$ is the new control input and $0 \le s_z(\eta) \in \mathbb{R} \le 1$ is a continuous non-decreasing function which is chosen to be asymptotically equal to 1 $\forall t \ge T_\eta$. As mentioned previously, the function $s_z(\eta)$ has the role of activating progressively and limiting the input $\tilde{u}$ during attitude control. Thus, at this stage, we have $s_z(\eta) \approx 1$, $\forall t \ge T_\eta$ and the double integrator $\ddot{z} = s_z(\eta)\tilde{u}$ can be controlled by the following saturated PD [26]

$$\tilde{u} = -\sigma_{\tilde{u}_{\max}}(k_{\tilde{u}1}\dot{z} + k_{\tilde{u}2}(z - z_d)) \tag{28}$$

where $(k_{\tilde{u}1}, k_{\tilde{u}2})$ are well-chosen positive gains.

From (28), we have $\lim_{t\to\infty} z = z_d$ and $\lim_{t\to\infty} \tilde{u} = 0$, which implies that $\exists T_z \ge T_\eta$ such that $\tilde{u} \approx 0$ $\forall t \ge T_z$.

C. Step 3. Horizontal Position Stabilization

Substituting (27) and (37) into (20), and considering that after a large finite time T_z, $\tilde{u} \approx 0$ and $s_h(\eta,z) \approx 1$, then the horizontal movement dynamics can be represented as follows

$$\begin{aligned} m\ddot{x} &= -mg\frac{\tan\theta}{\cos\phi} - \tan\theta\tan\phi f(\dot{\eta},\eta,\tilde{\tau}_\phi) \\ m\ddot{y} &= mg\tan\phi + \frac{1}{\cos\phi} f(\dot{\eta},\eta,\tilde{\tau}_\phi) \\ \ddot{\theta} &= -2\dot{\theta} - \theta + \tilde{\tau}_{\theta_{\text{trans}}} \\ \ddot{\phi} &= -2\dot{\phi} - \phi + \tilde{\tau}_{\phi_{\text{trans}}}. \end{aligned} \tag{29}$$

PROPOSITION 2 *There exists positive real constants* $(c_\theta, d_\theta, c_\phi, d_\phi)$ *satisfying* $c_\theta > d_\theta$ *and* $c_\phi > d_\phi$, *such that the system* (29) *is asymptotically stable considering the control law*

$$\begin{aligned} \tilde{\tau}_{\theta_{\text{trans}}} &= -\sigma_{c_\theta}(\dot{\theta} + 2\theta - \dot{x}/g) \\ &\quad - \sigma_{d_\theta}(\dot{\theta} + 3\theta - 3\dot{x}/g - x/g) \\ \tilde{\tau}_{\phi_{\text{trans}}} &= -\sigma_{c_\phi}(\dot{\phi} + 2\phi + \dot{y}/g) \\ &\quad - \sigma_{d_\phi}(\dot{\phi} + 3\phi + 3\dot{y}/g + y/g). \end{aligned} \tag{30}$$

The proof of Proposition 2 is developed in Appendix B.

V. EXPERIMENTAL SETUP AND RESULTS

In this section, we describe the experimental setup platform of the three-rotor helicopter including sensors and real-time architecture. The experimental results obtained using the proposed controller applied to the designed three-rotor aircraft are presented.

A. Platform Description

We have built a three-rotor aircraft as shown in Fig. 2. The parameters of the three-rotor craft are $m = 0.5$ kg, $l_1 = 0.07$ m, $l_2 = 0.24$ m, $l_3 = 0.33$ m.

For simplicity we have developed a Simulink-based platform using MATLAB Simulink xPC target (see Fig. 4). We have used the commercial radio Futaba to transmit the signals to the three-rotor aircraft. The radio joystick potentiometers have been connected through the data acquisitions cards, Advantech PCL-818HG (16 channels A/D) and Advantech PCL-726 (6 channels D/A) to the PC (xPC target module).

In order to measure the position (x,y,z) of the rotorcraft, we have used the 3D tracker system POLHEMUS. We have built a Simulink S-function for connecting the POLHEMUS via RS232 to the xPC target. The POLHEMUS system uses low-frequency magnetic transducing technology. It includes a

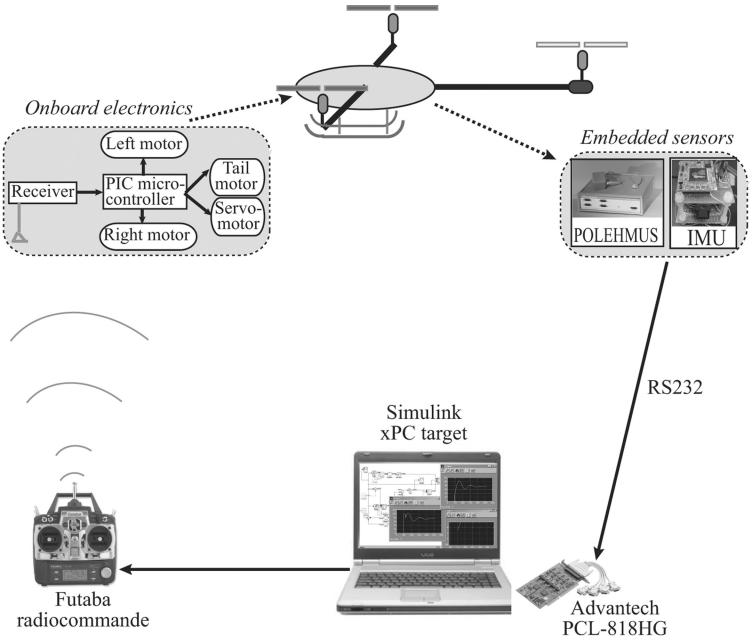

Fig. 4. Real-time architecture of platform.

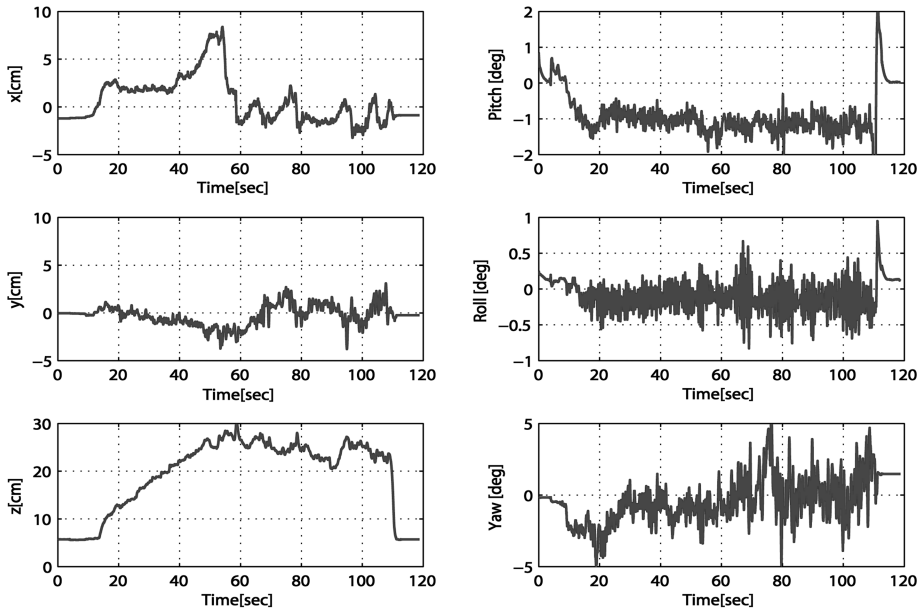

Fig. 5. Stabilization of position and attitude of rotorcraft.

system electronics unit (SEU), a power supply, one transmitter, and one small receiver. The SEU contains the hardware and software necessary to generate and sense the magnetic fields, compute position and orientation, and interface with the host computer via an RS-232 and USB. The transmitter contains electromagnetic coils enclosed in a molded plastic shell that emit the magnetic fields. The receiver contains electromagnetic coils that detect the magnetic fields emitted by the transmitter. The receiver's position and orientation are precisely measured by a small antenna.

Linear velocities are obtained using the approximation $\dot{\xi} = (\xi_t - \xi_{t-T})/T$ where ξ is the position and T is the sampling period. We have used a first-order low-pass filter to attenuate the linear velocity signal.

Our main interest involves the development of an embedded autopilot for small UAVs flying in outdoor environments. Therefore, for orientation sensing, we have used an onboard low-cost inertial measurement unit (IMU) that we have designed for small UAV navigation. The developed IMU contains three gyroscopes (ADXRS150) arranged orthogonally and a dual-axis micromachined silicon accelerometer (ADXL203). Gyroscopes and accelerometers data are fused in order to provide accurate measurements

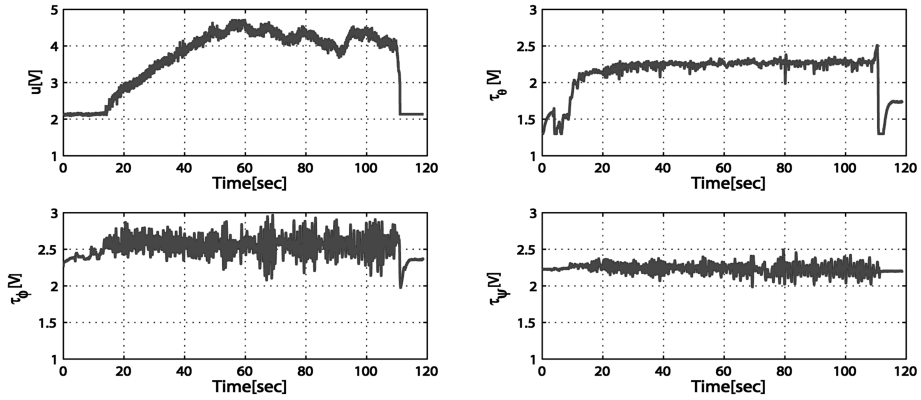

Fig. 6. Control inputs.

TABLE I
Controller Parameters

Controller Parameters	Values	Control Parameters	Values
$k_{\tilde{u}1}$	1	a_ψ	0.6
$k_{\tilde{u}2}$	2	b_ψ	0.29
$\tilde{u}_{\max}$	3	$c_\psi = d_\psi$	0
$a_\theta = a_\phi$	0.5	$c_\theta = c_\phi$	0.12
$b_\theta = b_\phi$	0.249	$d_\theta = d_\phi$	0.11

of the three angular rates $(\dot{\psi}, \dot{\theta}, \dot{\phi})$ and two angular positions (θ, ϕ).

The radio physical constraints are such that the control inputs have to satisfy the following inequalities

$$\begin{aligned} &0.40 \text{ V} < u < 4.70 \text{ V} \\ &0.40 \text{ V} < \tau_\phi < 4.50 \text{ V} \\ &0.40 \text{ V} < \tau_\theta < 4.16 \text{ V} \\ &0.40 \text{ V} < \tau_\psi < 4.15 \text{ V}. \end{aligned} \tag{31}$$

The real-time architecture of the platform is illustrated in Fig. 4. The rotorcraft evolves freely in a 3D space without any flying stand.

B. Flight Tests

The control goal is to perform the hover flight at the position $(x, y, z) = (0, 0, 25)$ while stabilizing the orientation $(\psi, \theta, \phi) = (0, 0, 0)$. The initial Euler angles and position are given by $\psi_0 \approx 0°$, $\theta_0 \approx 1°$, $\phi_0 \approx 0°$, $x_0 \approx 0$ cm, $y_0 \approx 0$ cm, and $z_0 \approx 5$ cm. Initial linear and angular velocities are set to zero.

The control law parameters are listed in Table I. The saturation levels are chosen according to (55), and the bounds on control torques are set to one (i.e., $\max(\tilde{\tau}_\psi) = \max(\tilde{\tau}_\theta) = \max(\tilde{\tau}_\phi) = 1$). The control signals (voltages) are then multiplied by "4" in order to exploit the whole range of the control energy without saturating the radio (31).

We can see that the altitude z follows the reference (Fig. 5). Concerning the position x and y, we observe a small deviation due to, among others, uncertainties and cable connections between the PC and the mini helicopter. The angles θ, ψ, and ϕ converge to zero and the control inputs are bounded (Figs. 5, 6). In all the figures, we note that the signals are corrupted by noise due to mechanical gears of motors and propellers.

VI. CONCLUSION

In this paper, we have described an original configuration for a small aerial vehicle and we have designed an autopilot for the stabilization task. The study provided in this paper has shown that a three-rotor aircraft without swashplate can provide the force and torque vectors required for normal flight.

The developed controller is based on the sum of saturating functions which aim at controlling sequentially the state variables in an appropriate order. The proposed control algorithm considers inputs amplitude constraints and deals with the coupling terms issued from tilting the tail rotor. In order to validate the three-rotor aircraft effectiveness and the autopilot performance, we have developed a Simulink-based platform and performed real-time experiments. We have obtained satisfying experimental results.

APPENDIX A

Let us choose the positive function $V_1 = \frac{1}{2}\dot{\eta}^T\dot{\eta}$, then its time derivative is given by

$$\dot{V}_1 = \dot{\eta}^T\tilde{\tau} = -\dot{\eta}^T(\sigma_a(\dot{\eta}) + \sigma_b(.) + s_h(\eta, z)\tilde{\tau}_{\text{trans}}).$$

Since $0 \le s_h(\eta, z) \le 1$, it is then clear that if $|\dot{\eta}| > a$ and $a > b + \max(\tilde{\tau}_{\text{trans}})$, then $\dot{V}_1$ is negative definite. Thus, $|\dot{\eta}|$ will decrease and will be bounded by a after a finite time T_1.

Therefore, $|\dot{\eta}| \le a$ and $\sigma_a(\dot{\eta}) = \dot{\eta}$, $\forall t \ge T_1$. Then, from (22)–(24) we can write

$$\ddot{\eta} + \dot{\eta} = -\sigma_b(\dot{\eta} + \eta) + s_h(\eta, z)\tilde{\tau}_{\text{trans}}. \tag{32}$$

Then, by defining $z_2 = (z_{2_\phi}, z_{2_\theta}, z_{2_\psi})^T$ as

$$z_2 = \dot{\eta} + \eta \tag{33}$$

and by evaluating its first time derivative

$$\dot{z}_2 = -\sigma_b(z_2) + s_h(\eta, z)\tilde{\tau}_{\text{trans}} \tag{34}$$

we obtain a system similar to the previous one. By following the same methodology, we can prove that there exists $T_2 \geq T_1$ such that $\forall t \geq T_2$, $|z_2| \leq b$ for $b > \max(\tilde{\tau}_{\text{trans}})$. Therefore, $\sigma_b(z_2)$ will operate in its linear region $\forall t \geq T_2$ and system (23) becomes

$$\ddot{\eta} = -2\dot{\eta} - \eta + s_h(\eta, z)\tilde{\tau}_{\text{trans}}, \qquad \forall \quad t \geq T_2. \tag{35}$$

Since $\forall t \geq T_2$, $|z_2| \leq b$, then the solution of the differential equation (33) satisfies (see [12])

$$|\eta| \leq b, \qquad \forall \quad t \geq T_\eta \geq T_2. \tag{36}$$

This ends the proof for the first part (attitude boundedness) of Proposition 1.

From (23) and (35), we have

$$\ddot{\eta} = -2\dot{\eta} - \eta + s_h(\eta, z)\tilde{\tau}_{\text{trans}}. \tag{37}$$

Since $s^2 + 2s + 1$ is a stable polynomial, then $(\dot{\eta}, \eta)$ will converge exponentially to zero when $\tilde{\tau}_{\text{trans}} \equiv 0$.

APPENDIX B

Let us first, consider the subsystem in (29) describing the longitudinal translation dynamics

$$\begin{aligned} m\ddot{x} &= -mg\frac{\tan\theta}{\cos\phi} - \tan\theta\tan\phi f(\dot{\eta}, \eta, \tilde{\tau}_\phi) \\ \ddot{\theta} + 2\dot{\theta} + \theta &= \tilde{\tau}_{\theta_{\text{trans}}}. \end{aligned} \tag{38}$$

By using the control law in (30), we will successively bound $\dot{x}$ and x and we will prove that the state variables $(\dot{x}, x, \dot{\theta}, \theta)$ will converge to zero if the saturation levels are chosen appropriately.

States Boundedness: Let us define z_{3_θ} as

$$z_{3_\theta} = \dot{\theta} + 2\theta - \dot{x}/g. \tag{39}$$

By recalling (38), the time derivative of z_{3_θ} is given by

$$\dot{z}_3 = -\sigma_{c_\theta}(z_{3_\theta}) - \sigma_{d_\theta}(z_{4_\theta}) + h(\dot{\eta}, \eta, \tilde{\tau}_\phi) \tag{40}$$

with

$$\begin{aligned} h(\dot{\eta}, \eta, \tilde{\tau}_\phi) &= \left(\frac{\tan\theta}{\cos\phi} - \theta\right) \\ &\quad + \frac{1}{mg}\tan\theta\tan\phi f(\dot{\eta}, \eta, \tilde{\tau}_\phi) \\ \tilde{\tau}_{\theta_{\text{trans}}} &= -\sigma_{c_\theta}(z_{3_\theta}) - \sigma_{d_\theta}(z_{4_\theta}) \end{aligned} \tag{41}$$

and z_{4_θ} will be defined later. Since $(\dot{\eta}, \eta, \tilde{\tau}_\phi)$ are bounded (see Appendix A), then the function $|h|$ is bounded by some small positive constant[4] $m_\theta(a, b)$.

[4]From (21) and (41), we can show that $m_\theta \leq 0.05$ for $b_\theta = b_\phi \leq 0.4$.

We continue this procedure by defining a positive definite function $V_3 = \frac{1}{2}z_{3_\theta}^2$. Then,

$$\dot{V}_3 = -z_{3_\theta}(-\sigma_{c_\theta}(z_{3_\theta}) - \sigma_{d_\theta}(z_{4_\theta}) + h(\dot{\eta}, \eta, \tilde{\tau}_\phi)). \tag{42}$$

As previously, we can see that the time derivative of V_3 is negative definite if $|z_{3_\theta}| > c_\theta$ and $c_\theta > d_\theta + m_\theta$. Thus, $\exists T_3 \geq T_z$ such that the variable $|z_{3_\theta}|$ will decrease until it enters and remains in the domain $[-c_\theta, c_\theta]$ for all $t \geq T_3$. Therefore, $\sigma_{c_\theta}(z_{3_\theta}) = z_{3_\theta}$ for all $t \geq T_3$. From (39), we deduce that $\dot{x}$ is bounded.

Now, system (40) can be written as follows

$$\dot{z}_3 + z_{3_\theta} = -\sigma_{d_\theta}(z_{4_\theta}) + h(\dot{\eta}, \eta, \tilde{\tau}_\phi). \tag{43}$$

Finally, we define

$$z_{4_\theta} = z_{3_\theta} + \theta - 2\dot{x}/g - x/g. \tag{44}$$

By differentiating this equation with respect to the time and recalling (38), (39), (41), and (43), we obtain

$$\dot{z}_4 = -\sigma_{d_\theta}(z_{4_\theta}) + 3h(\dot{\eta}, \eta, \tilde{\tau}_\phi). \tag{45}$$

This system is similar to the previous one in (40), so we can deduce that there exists $T_4 \geq T_3$ such that, if $d_\theta > 3m_\theta$, then $|z_{4_\theta}| \leq d_\theta$ $\forall t \geq T_4$. Therefore,

$$\dot{z}_4 + z_{4_\theta} = 3h(\dot{\eta}, \eta, \tilde{\tau}_\phi). \tag{46}$$

From (44), we deduce that x is bounded.

Convergence Analysis: In this section, we prove that all the states $(\dot{\theta}, \theta, \dot{x}, x)$ will converge to zero even in the presence of the coupling term $h(\dot{\eta}, \eta, \tilde{\tau}_\phi)$. The global asymptotic stability is ensured by a convenient choice of the saturation levels $(a_\theta, b_\theta, c_\theta, d_\theta)$.

After solving and analyzing the differential equation (46), we find that its solution satisfies the inequality below

$$|z_{4_\theta}| \leq 3\left|\frac{\tan\theta}{\cos\phi} - \theta\right| + 3\frac{1}{mg}|\tan\theta\tan\phi f(\dot{\eta}, \eta, \tilde{\tau}_\phi)|. \tag{47}$$

From (43), we also deduce that

$$|z_{3_\theta}| \leq 4\left|\frac{\tan\theta}{\cos\phi} - \theta\right| + 4\frac{1}{mg}|\tan\theta\tan\phi f(\dot{\eta}, \eta, \tilde{\tau}_\phi)|. \tag{48}$$

Similarly, from (34) we obtain

$$|z_{2_\theta}| \leq 7\left|\frac{\tan\theta}{\cos\phi} - \theta\right| + \frac{7}{mg}|\tan\theta\tan\phi f(\dot{\eta}, \eta, \tilde{\tau}_\phi)|. \tag{49}$$

Finally, we also conclude from (33) that

$$|\theta| \leq 7\left|\frac{\tan\theta}{\cos\phi} - \theta\right| + \frac{7}{mg}|\tan\theta\tan\phi f(\dot{\eta}, \eta, \tilde{\tau}_\phi)|. \tag{50}$$

Now, we will prove that θ converges to zero if the saturation level b_θ is small enough.

By recalling (36) and (50), one has

$$|\theta| - 7\left|\frac{\tan\theta}{\cos\phi} - \theta\right| \le \frac{7}{mg}|\tan\theta\tan\phi f(\dot\eta,\eta,\tilde\tau_\phi)| \qquad |\theta| \le b_\theta. \tag{51}$$

Let us notice that $\tan\theta$ and θ have the same sign, and $|\tan\theta| \ge |\theta|$ for $|\theta| \le b_\theta < \pi/2$ which implies that $|\tan\theta/\cos\phi| \ge |\theta|$ since $0 < |\cos\phi| \le 1$.

We conclude from these remarks that

$$\left|\frac{\tan\theta}{\cos\phi} - \theta\right| = \frac{|\tan\theta|}{|\cos\phi|} - |\theta|. \tag{52}$$

Substituting (52) into (51), we obtain

$$8|\theta| - 7\frac{|\tan\theta|}{|\cos\phi|} \le \frac{7}{mg}|\tan\theta\tan\phi f(\dot\eta,\eta,\tilde\tau_\phi)| \qquad |\theta| \le b_\theta. \tag{53}$$

By studying and plotting in MATLAB® the first inequality in (53), we find that its solution is $\{|\theta| \in 0 \cup [\sim 0.4, (\pi/2)[\}$. Therefore, if we choose $b_\theta < 0.4$, then the only possible solution of (53) is $\{\theta = 0\}$.

Thus, from (47)–(49), we have $(z_{2_\theta}, z_{3_\theta}, z_{4_\theta}) \to (0,0,0)$. From (33), we get $\dot\theta \to 0$. Finally, from (39) and (44), it follows that $\dot x \to 0$ and $x \to 0$. Thus, $\exists T_5 \ge T_4$ such that $(\dot\theta, \theta, \dot x, x) \approx (0,0,0,0)$, $\forall t \ge T_5$.

Let us rewrite the constraints on saturation levels

$$\begin{aligned} &a_\theta + b_\theta + c_\theta + d_\theta \le \tilde\tau_{\theta\max} \\ &a_\theta > b_\theta + c_\theta + d_\theta \\ &b_\theta > c_\theta + d_\theta \\ &b_\theta < \pi/2 \\ &c_\theta > d_\theta + m_\theta \\ &d_\theta > 3m_\theta. \end{aligned} \tag{54}$$

A simple and convenient selection consists in choosing

$$\begin{aligned} &a_\theta = (\tilde\tau_{\theta\max} - \delta)/2 \\ &b_\theta \le (a_\theta - \delta)/2 \qquad \text{and} \qquad b_\theta < 0.4 \\ &\qquad \text{(convergence condition)} \\ &c_\theta = (b + m_\theta + \delta)/2 \\ &3m_\theta < d_\theta < c_\theta - m_\theta \end{aligned} \tag{55}$$

where δ is an arbitrary small positive constant and $\tilde\tau_{\theta\max}$ is the maximum magnitude of $\tilde\tau_\theta$.

Now, let us show that the remaining subsystem in (29), describing the lateral movement dynamics, can be stabilized using the same procedure.

Since $(\dot\theta, \theta, \dot x, x) \approx (0,0,0,0)$, $\forall t \ge T_5$, then from (21), we have $f(\dot\eta,\eta,\tilde\tau_\phi)$ is arbitrarily small enough. Then, the subsystem describing the lateral movement dynamics in (29) reduces to

$$m\ddot y = mg\tan\phi, \qquad \ddot\phi + 2\dot\phi + \phi = \tilde\tau_{\phi_{\text{trans}}}. \tag{56}$$

This subsystem is similar to (38), and using the previous analysis, it is easy to show that the control law $\tilde\tau_{\phi_{\text{trans}}}$ in (30) asymptotically stabilizes the subsystem formed by $(\dot\phi, \phi, \dot y, y)$ in (56).

REFERENCES

[1] Buskey, G., Wyeth, G., and Roberts, J.
Autonomous helicopter hover using an artificial neural network.
In *Proceedings of the IEEE International Conference on Robotics and Automation*, Seoul, Korea, 2001, 1635–1640.

[2] Shim, H., Koo, T. J., Hoffman, F., and Sastry, S.
A comprehensive study of control design of an autonomous helicopter.
In *Proceedings of the 37th IEEE Conference on Decision and Control*, Tampa, FL, 1998, 3653–3658.

[3] Bouabdallah, S., and Siegwart, R.
Backstepping and sliding-mode techniques applied to an indoor micro quadrotor.
In *Proceedings of the IEEE International Conference on Robotics and Automation*, Barcelona, Spain, Apr. 2005, 2259–2264.

[4] Kendoul, F., Fantoni, I., and Lozano, R.
Modeling and control of a small autonomous aircraft having two tilting rotors.
IEEE Transactions on Robotics, **22**, 6 (Dec. 2006), 1297–1302.

[5] Sepulcre, R., Jankovic, M., and Kokotovic, P.
Constructive Nonlinear Control.
London: Springer-Verlag, 1997.

[6] Johnson, E. N., and Kannan, S. K.
Adaptive flight control for an autonomous unmanned helicopter.
AIAA Guidance, Navigation and Control Conference, 2002, paper AIAA-2002-4439.

[7] Hauser, J., Sastry, S., and Meyer, G.
Nonlinear control design for slightly nonminimum phase systems: Application to V/STOL aircraft.
Automatica, **28**, 4 (1992), 665–679.

[8] Fantoni, I., and Lozano, R.
Non-Linear Control for Underactuated Mechanical Systems (Communications and Control Engineering Series).
Springer-Verlag, 2002.

[9] Lauvdal, T., and Murray, R. M.
Stabilization of a pitch axis flight control experiment with input rate saturation.
Presented at the AIAA Conference on Guidance, Navigation, and Control, 1997.

[10] Teel, A. R.
Global stabilisation and restricted tracking for multiple integrators with bounded controls.
Systems and Control Letters, **18** (1992), 165–171.

[11] Castillo, P., Dzul, A., and Lozano, R.
Real-time stabilization and tracking of a four rotor mini-rotorcraft.
IEEE Transactions on Control Systems Technology, **12**, 4 (July 2004), 510–516.

[12] Lozano, R., Castillo, P., and Dzul, A.
Global stabilization of the PVTOL: Real-time application to a mini-aircraft.
International Journal of Control, **77**, 8 (May 2004), 735–740.

[13] Vachtsevanos, G., Tang, L., Drozeski, G., and Gutierrez, L.
From mission planning to flight control of unmanned aerial vehicles: Strategies and implementation tools.
Annual Reviews in Control, (2005).

[14] Ollero, A., and Merino, L.
Control and perception techniques for aerial robotics.
Annual Reviews in Control, **28** (2004), 167–178.

[15] Sussmann, J. H., Sontag, D. E., and Yang, Y.
A general result on the stabilization of linear systems using bounded controls.
IEEE Transactions on Automatic Control, **39**, 12 (Dec. 1994), 2411–2425.

[16] Vilchis, J. A., Brogliato, B., Dzul, A., and Lozano, R.
Nonlinear modelling and control of helicopters.
Automatica, **39**, 9 (Sept. 2003), 1583–1596.

[17] Beji, L., and Abichou, A.
Trajectory generation and tracking of a mini-rotorcraft.
In *Proceedings of the International Conference on Robotics and Automation*, Barcelona, Spain, Apr. 2005, 2629–2634.

[18] Tayebi, A., and McGilvray, S.
Attitude stabilization of a four-rotor aerial robot.
In *43rd IEEE Conference on Decision and Control*, Atlantis, Paradise Island, Bahamas, Dec. 2004, 1216–1221.

[19] Unmanned aerial vehicles roadmap.
Office of the Secretary of Defense, Washington, D.C., 2001.

[20] Dzul, A., Lozano, R., and Castillo, P.
Adaptive control for a radio-controlled helicopter in a vertical flying stand.
International Journal of Adaptive Control and Signal Processing, **18**, 5 (June 2004), 473–485.

[21] Castillo, P., Lozano, R., and Dzul, A.
Modelling and Control of Mini-Flying Machines.
Springer-Verlag, 2005.

[22] Prouty, R. W.
Helicopter Performance, Stability, and Control.
K. P. Compagny, Ed., Malabar, Florida, 1995.

[23] Johnson, W.
Helicopter Theory.
N. P. U. P. Princeton, Ed., 1980.

[24] Etkin, B.
Dynamics of Flight.
J. Wiley & Sons, Ed., New York, 1959.

[25] McCormick, B. W.
Aerodynamics Aeronautics and Flight Mechanics.
J. Wiley & Sons, Ed., New York, 1995.

[26] Sussmann, J. H., and Yang, Y.
On the stabilizability of multiple integrators by means of bounded feedback controls.
In *Proceedings of the 30th IEEE Conference on Decision and Control*, Brighton, UK, 1991.

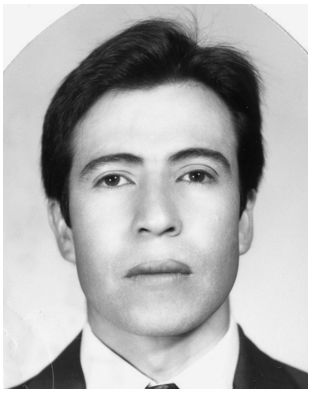

Sergio Salazar-Cruz received the B.E. degree from the Universidad Autónoma de Puebla México in 1992, the M.S. degree from the CINVESTAV México in 1994 and the Ph.D. degree from the Université de Technologie de Compiègne France in 2005.

He is currently a researcher at Instituto de Investigaciones Eléctricas in Cuernavaca México. His research focuses on the development of autonomous vehicles.

Farid Kendoul was born in Béjaia, Algeria in 1980. He received the Engineer Diploma in robotics and mechatronic, and the Master's Degree in automatic control from the University of Technology of Compiègne, France, in 2004. He is currently working toward the Ph.D. Degree at the University of Technology of Compiègne, and he is a member of the UAV Group in the Heudiasyc Laboratory.

His research interests are modelling and control of unmanned aerial vehicles, flight control and guidance, adaptive and nonlinear control, computer vision and insect-inspired control of small flying machines. His current research focuses on the development of an adaptive vision-based autopilot for small rotorcraft control and 3D navigation.

Rogelio Lozano (M'94) was born in Monterrey Mexico, on July 12, 1954. He received the B.S. degree in electronic engineering from the National Polytechnic Institute of Mexico in 1975, the M.S. degree in electrical engineering from Centro de Investigación y de Estudios Avanzados (CINVESTAV), Mexico in 1977, and the Ph.D. degree in automatic control from Laboratoire d'Automatique de Grenoble, France, in 1981.

He joined the Department of Electrical Engineering at CINVESTAV, Mexico, in 1981 where he worked until 1989. He was head of the Section of Automatic Control from June 1985 to August 1987. He has held visiting positions at the University of Newcastle, Australia, from November 1983 to November 1984, NASA Langley Research Center, VA, from August 1987 to August 1988, and Laboratoire d'Automatique de Grenoble, France, from February 1989 to July 1990. Since 1990 he is a CNRS research director at the University of Technology of Compiègne, France. He was promoted to 1st class CNRS research director in 1997. He is head of the Laboratory Heudiasyc, UMR 6599 CNRS-UTC since January 1995. His research interests are in adaptive control of linear, nonlinear systems, robot manipulators, passive systems, teleoperation and unmanned aerial vehicles.

Dr. Lozano was Associate Editor of *Automatica* in the period 1987–2000 and of *International Journal of Adaptive Control and Signal Processing* since 1993.

Isabelle Fantoni (M'02) was born in Le Mans, France, on January 31, 1973. She graduated from the University of Technology of Compiègne (UTC), in France and received the Master of Sciences in electronic system design at the University of Cranfield in England (double degree), both in 1996. She received the Master in control systems, in 1997 and the Ph.D. degree, in 2000 from the University of Technology of Compiègne, in France.

Since October 2001, she has been a permanent researcher at Heudiasyc Laboratory, UTC, in Compiègne, France, employed by the French National Foundation for Scientific Research (CNRS). Her research interests include nonlinear control, underactuated mechanical systems, modelling and control for unmanned aerial vehicles, and computer vision for navigation of aerial vehicles.